half-space Green's function. The image reconstruction problem is first transformed into a nonlinear optimization problem, and then optimized by the modified fireworks algorithm. Such a transformation from a nonlinear equation to anther optimization problem will make the flowchart of microwave imaging easy and straightforward. This transformation also makes the image reconstruction problem easy to utilize modern optimization techniques. With the use of our modified fireworks algorithm, the reconstructed target shape is accurate and the convergence is fast. The fireworks algorithm based procedures of this study can be applied to many other nonlinear electromagnetic problems.

ACKNOWLEDGMENTS

The author would like to acknowledge the financial support of the Ministry of Science and Technology, Taiwan, under contract number of MOST 106-2221-E-006-117. The author would also like to express their sincere gratitude to National Center for High-performance Computing, Taiwan, for supporting the computing hardware and software.

ORCID

Kun-Chou Lee http://orcid.org/0000-0002-7867-4860

REFERENCES

[1] Islam MA, Kiourti A, Volakis JL. A modified Gauss-Newton algorithm for fast microwave imaging using near-field probes. *Microw Opt Technol Lett.* 2017;59(6):1394–1400.

[2] Liu Y, Zhao Z, Zhu X, Yang W, Nie Z, Liu QH. A diagonalized improved subspace-based optimization method for solving 2-D inverse scattering problems. *Microw Opt Technol Lett.* 2017;59(8):2089–2095.

[3] AhadiIsa MM, Saripan MI, Hasan WZW. Three dimensions localization of tumors in confocal microwave imaging for breast cancer detection. *Microw Opt Technol Lett.* 2015;57(12):2917–2929.

[4] Moriyama T, Takenaka T. Inverse scattering approach with measurement of only total electric field. *Microw Opt Technol Lett.* 2015;57(1):137–141.

[5] Roger A. Newton-Kantorovitch algorithm applied to an electromagnetic inverse problem. *IEEE Trans Antennas Propag.* 1981;29(2):232–238.

[6] Kirsch A, Kress R, Monk P, Zinn A. Two methods for solving the inverse acoustic scattering problem. *Inverse Probl.* 1988;4(3):749–770.

[7] Colton D, Monk P. A new method for solving the inverse scattering problem for acoustic waves in an inhomogeneous medium. *Inverse Probl.* 1989;5(6):1013–1026.

[8] Otto GP, Chew WC. Microwave inverse scattering-local shape function imaging for improved resolution of strong scatterers. *IEEE Trans Microw Theory Tech.* 1994;42:137–141.

[9] Hettlich F. Two method for solving an inverse conductive scattering problem. *Inverse Probl.* 1994;10(2):375–385.

[10] Lee KC. A neural network based model for the two dimensional microwave imaging of cylinders. *Int J RF Microw Comput-Aid Eng.* 2004;14(5):398–403.

[11] Chiu CC, Kiang YW. Inverse scattering of a buried conducting cylinder. *Inverse Probl.* 1991;7:187–202.

[12] Chiu CC, Chen CH, Fan YS. Image reconstruction of a buried conductor by modified particle swarm optimization. *IETE J Res.* 2012;58(4):284–291.

[13] Tan Y, Zhu Y. Fireworks algorithm for optimization. In: International Conference on Swarm Intelligence (ICSI 2010), Part I; 2010, pp. 355–364, Beijing, China.

[14] Robinson J, Rahmat-Samii Y. Particle swarm optimization in electromagnetics. *IEEE Trans Antennas Propag.* 2004;52(2):397–407.

[15] Lee K-C. Inverse scattering of a conducting cylinder in free space by modified fireworks algorithm. *Prog Electromagn Res M.* 2017;59:135–146.

[16] Balanis CA. *Advanced Engineering Electromagnetics*. New York: Wiley; 1989.

[17] Wait JR. *Electromagnetic Waves in Stratified Media*. New York: Macmillan; 1962.

[18] Harrington RF. *Field Computation by Moment Methods*. New York: Macmillan; 1968.

[19] Oppenheim AV, Schafer RW, Buck JR. *Discrete-Time Signal Processing*. 2nd ed. New Jersey: Prentice Hall; 1999.

[20] Butler CM, Xu XB, Glisson AW. Current induced on a conducting cylinder located near the planar interface between two semi-infinite half-spaces. *IEEE Trans Antennas Propag.* 1985;33:616–624.

How to cite this article: Lee K-C. Microwave imaging of a conducting cylinder buried in a lossless half space by modified fireworks algorithm. *Microw Opt Technol Lett*. 2018;60:1374–1381. https://doi.org/10.1002/mop.31159

Received: 27 September 2017

DOI: 10.1002/mop.31166

A butterfly-based direct solver using hierarchical LU factorization for Poggio-Miller-Chang-Harrington-Wu-Tsai equations

Han Guo[1] | Yang Liu[1] | Jun Hu[2] | Eric Michielssen[1]

[1] Department of Electrical Engineering and Computer Science, University of Michigan, Ann Arbor, Michigan 48109

[2]Department of Microwave Engineering, University of Electronic Science and Technology of China, Chengdu, Sichuan 611731, China

Correspondence
Yang Liu, Department of Electrical Engineering and Computer Science, University of Michigan, Ann Arbor, MI 48109.
Email: liuyangz@umich.edu

Abstract

A butterfly-based hierarchical LU factorization scheme for solving the PMCHWT equations for analyzing scattering from homogenous dielectric objects is presented. The proposed solver judiciously re-orders the discretized integral operator and butterfly-compresses blocks in the operator and its LU factors. The observed memory and CPU complexities scale as $O(N \log^2 N)$ and $O(N^{1.5} \log N)$, respectively. The proposed solver is applied to the analyses of scattering several large-scale dielectric objects.

KEYWORDS

butterfly scheme, fast direct solver, homogenous dielectrics, integral equation, Poggio-Miller-Chang-Harrington-Wu-Tsai equation (PMCHWT), scattering analysis

1 | INTRODUCTION

The analysis of electromagnetic scattering from large-scale (piecewise) homogenous dielectric-magnetic objects oftentimes is performed using fast multipole-accelerated Poggio-Miller-Chang-Harrington-Wu-Tsai (PMCHWT) integral equation (IE) solvers.[1,2] Unfortunately, these iterative methods suffer from poor convergence when the object under study supports high-Q resonances or is discretized via dense meshes. They also become inefficient when applied to problems involving multiple excitations or requiring partial updates of discretized IE operators, further termed interaction matrices.

Fast direct solvers oftentimes outperform iterative ones under these conditions. With few exceptions, present direct solvers approximate off-diagonal blocks of interaction matrices and their "inverses" (e.g., LU factors and inverse decompositions leveraging H-matrix, hierarchically semi-separable matrix, and skeletonization techniques) using low-rank (LR) products.[3–9] These solvers exhibit quasi-linear CPU and memory requirements when applied to electrically small[3,10] and structured[11–14] objects. However, when used for analyzing scattering from electrically large and arbitrarily-shaped objects, their CPU and memory requirements deteriorate to $O(N^{\alpha} \log^{\beta} N)$ ($\alpha = 2.0 \sim 3.0$, $\beta \geq 1$) and $O(N^{\alpha} \log N)$ ($\alpha = 1.3 \sim 2.0$) , as off-diagonal blocks of interaction matrices and their inverses are no longer LR compressible.

Recently, a new class of direct solvers leveraging butterfly compression schemes[15–18] was developed.[19–21] Butterfly schemes represent judiciously selected submatrices in off-diagonal blocks of interaction matrices (that are themselves LR incompressible) and their inverses in terms of LR products. The CPU and memory requirements of butterfly-based direct solvers for analyzing scattering from perfect electrically conducting (PEC) objects were estimated and experimentally validated to be $O(N^{1.5} \log N)$ and $O(N \log^2 N)$, irrespective of the object's shape and size.[21]

This letter extends the above-referenced solver for PEC scatterers to homogeneous dielectric-magnetic objects. Specifically, it introduces a fast butterfly-enhanced hierarchical LU scheme for solving the PMCHWT equations. Butterfly compression is applied to blocks of a judiciously reordered PMCHWT interaction matrices, effectively combining four blocks in the original matrix into one that models a single (admissible) source-observer pair. The solver is applied to the analysis of scattering from a sphere, a NASA almond, and a helicopter model involving one million unknowns. Its CPU and memory requirements are observed to scale as $O(N^{1.5} \log N)$ and $O(N \log^2 N)$, respectively.

2 | FORMULATION

2.1 | PMCHWT equations

Let Γ denote an arbitrarily-shaped closed surface with outward pointing normal $\hat{\boldsymbol{n}}$. The exterior and interior of Γ henceforth are termed regions 1 and 2. Region $i = 1,2$ has constant permittivity and permeability ε_i and μ_i, respectively. Time-harmonic electromagnetic fields $\{\boldsymbol{E}^{\text{inc}}(\boldsymbol{r}), \boldsymbol{H}^{\text{inc}}(\boldsymbol{r})\}$ with angular frequency ω produced by sources in region 1 impinge on Γ. Total electromagnetic fields $\{\boldsymbol{E}(\boldsymbol{r}), \boldsymbol{H}(\boldsymbol{r})\}$ are composed of incident and scattered fields, and relate to equivalent electric and magnetic currents $\boldsymbol{J}(\boldsymbol{r}) = \hat{\boldsymbol{n}} \times \boldsymbol{H}(\boldsymbol{r})$ and $\boldsymbol{M}(\boldsymbol{r}) = \boldsymbol{E}(\boldsymbol{r}) \times \hat{\boldsymbol{n}}$ on Γ that satisfy the PMCHWT equations

$$\mathcal{T}_1[\eta_1 \boldsymbol{J}](\boldsymbol{r}) + \frac{\eta_2}{\eta_1}\mathcal{T}_2[\eta_1 \boldsymbol{J}](\boldsymbol{r}) - \mathcal{K}_1[\boldsymbol{M}](\boldsymbol{r}) - \mathcal{K}_2[\boldsymbol{M}](\boldsymbol{r}) = -\hat{\boldsymbol{n}} \times \boldsymbol{E}^{\text{inc}}(\boldsymbol{r}) \tag{1}$$

$$\mathcal{K}_1[\eta_1 \boldsymbol{J}](\boldsymbol{r}) + \mathcal{K}_2[\eta_1 \boldsymbol{J}](\boldsymbol{r}) + \mathcal{T}_1[\boldsymbol{M}](\boldsymbol{r})\frac{\eta_1}{\eta_2}\mathcal{T}_2[\boldsymbol{M}](\boldsymbol{r}) = -\eta_1 \hat{\boldsymbol{n}} \times \boldsymbol{H}^{\text{inc}}(\boldsymbol{r}). \tag{2}$$

Here, $\eta_i = \sqrt{\mu_i/\varepsilon_i}$ is the wave impedance in region i, and the operators $\mathcal{T}_i$ and $\mathcal{K}_i$ are

$$\mathcal{T}_i[\boldsymbol{F}](\boldsymbol{r}) = ik_i\eta_i\hat{\boldsymbol{n}} \times \int_{\Gamma} d\boldsymbol{r}' \boldsymbol{F}(\boldsymbol{r}') \cdot \left(\boldsymbol{I} - \frac{\nabla\nabla'}{k_i^2}\right) g_i(\boldsymbol{r}, \boldsymbol{r}') \tag{3}$$

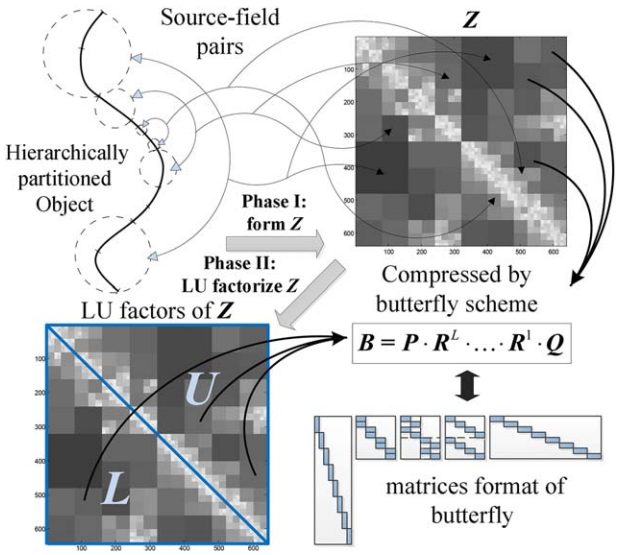

FIGURE 1 Matrix format of butterfly-based direct solver [Color figure can be viewed at wileyonlinelibrary.com]

$$\mathcal{K}_i[\boldsymbol{F}](\boldsymbol{r}) = -\hat{\boldsymbol{n}} \times P.V. \int_\Gamma d\boldsymbol{r}' \boldsymbol{F}(\boldsymbol{r}') \times \nabla' g_i(\boldsymbol{r}, \boldsymbol{r}') \tag{4}$$

where $\boldsymbol{I}$ is the identity dyad, *P. V.* denotes Cauchy principal value, and $k_i = \omega\sqrt{\varepsilon_i \mu_i}$, and $g_i(\boldsymbol{r},\boldsymbol{r}') = \exp(ik_i R)/(4\pi R)$ with $R = |\boldsymbol{r} - \boldsymbol{r}'|$ are the wavenumber and Green's function for region i, respectively.

To numerically solve Equations 1 and 2, currents $\eta_1 \boldsymbol{J}(\boldsymbol{r})$ and $\boldsymbol{M}(\boldsymbol{r})$ are discretized using N' Rao-Wilton-Glisson (RWG) basis functions $\boldsymbol{f_n}(\boldsymbol{r})$ as[22]

$$\eta_1 \boldsymbol{J}(\boldsymbol{r}) = \sum_{n=1}^{N'} I_n^J \boldsymbol{f}_n(\boldsymbol{r}) \tag{5}$$

$$\boldsymbol{M}(\boldsymbol{r}) = \sum_{n=1}^{N'} I_n^M \boldsymbol{f}_n(\boldsymbol{r}). \tag{6}$$

Here, I_n^J and I_n^M are electric and magnetic current expansion coefficients associated with $\boldsymbol{f_n}(\boldsymbol{r})$. Inserting Equations 5 and 6 into Equations 1 and 2 and testing the resulting equation with $\hat{\boldsymbol{n}} \times \boldsymbol{f_n}(\boldsymbol{r})$ yields the following $N \times N$ with $N = 2N'$ linear system of equations:

$$\begin{bmatrix} \boldsymbol{T}_1 + \frac{\eta_2}{\eta_1} \boldsymbol{T}_2 & -\boldsymbol{K}_1 - \boldsymbol{K}_2 \\ \boldsymbol{K}_1 + \boldsymbol{K}_2 & \boldsymbol{T}_1 + \frac{\eta_1}{\eta_2} \boldsymbol{T}_2 \end{bmatrix} \begin{bmatrix} \boldsymbol{I}^J \\ \boldsymbol{I}^M \end{bmatrix} = \begin{bmatrix} \boldsymbol{V}^E \\ \boldsymbol{V}^H \end{bmatrix}. \tag{7}$$

Here, the n^{th} entries of $\boldsymbol{I}^J$ and $\boldsymbol{I}^M$ are I_n^J and I_n^M, respectively. The m^{th} entries of $\boldsymbol{V}^E$ and $\boldsymbol{V}^H$, $m = 1,\ldots,N'$, are

$$V_m^E = -\langle \hat{\boldsymbol{n}} \times \boldsymbol{f}_m(\boldsymbol{r}), \hat{\boldsymbol{n}} \times \boldsymbol{E}^{\text{inc}}(\boldsymbol{r}) \rangle \tag{8}$$

$$V_m^H = -\langle \hat{\boldsymbol{n}} \times \boldsymbol{f}_m(\boldsymbol{r}), \eta_1 \hat{\boldsymbol{n}} \times \boldsymbol{H}^{\text{inc}}(\boldsymbol{r}) \rangle \tag{9}$$

where $\langle \cdot,\cdot \rangle$ denotes the standard inner product. The $(m, n)^{\text{th}}$ elements of the interaction matrix follow from

$$T_{i,mn} = \langle \hat{\boldsymbol{n}} \times \boldsymbol{f}_m(\boldsymbol{r}), \mathcal{T}_i[\boldsymbol{f}_n](\boldsymbol{r}) \rangle \tag{10}$$

$$K_{i,mn} = \langle \hat{\boldsymbol{n}} \times \boldsymbol{f}_m(\boldsymbol{r}), \mathcal{K}_i[\boldsymbol{f}_n](\boldsymbol{r}) \rangle \tag{11}$$

The CPU and memory costs for directly solving Equation 7 via Gaussian elimination or LU factorization scale as $O(N^3)$ and $O(N^2)$, respectively. Below, a butterfly-based hierarchical LU factorization scheme that reduces these requirements to $O(N^{1.5} \log N)$ and $O(N \log^2 N)$ is outlined. The scheme consists of two steps: filling/compressing and hierarchical LU factorization of the interaction matrix.

2.2 | Matrix filling/compression

The solver constructs a compressed representation of the interaction matrix in Equation 7 via (i) recursive matrix decomposition and (ii) butterfly compression of off-diagonal blocks.

Step (i) recursively bisects Γ L^{M} times until the finest-level subscatterers contain $O(1)$ basis functions. At level $1 \le l \ge L^{\text{M}}$, there are 2^l level $-l$ subscatterers, each containing roughly $N'/2^l$ basis functions. Two level $-l$ subscatterers constitute a far-field pair if their geometric centers are separated by at least $1 < \chi < 4$ times the sum of their circumscribing radii and their parent subscatterers do not form a far-field pair; two level $-L^{\text{M}}$ subscatterers that do not form a far-field pair constitute a near-field pair.

There are two unknowns (I_n^J and I_n^M) and two tested fields (V_n^E and V_n^H) associated with each function $\boldsymbol{f_n}(\boldsymbol{r})$. It follows there are four blocks in Equation 7 associated with each subscatterer pair. To efficiently compress all blocks associated with one far-field pair, rows, and columns in the interaction matrix in Equation 7 are permuted, resulting in the following system of equations:

$$\boldsymbol{Z}\boldsymbol{I} = \boldsymbol{V}. \tag{12}$$

Here, $\boldsymbol{I} = (I_1^J, I_1^M, \ldots, I_{N'}^J, I_{N'}^M)^T$, $\boldsymbol{V} = (V_1^E, V_1^M, \ldots, V_{N'}^E, V_{N'}^M)^T$ and

$$\boldsymbol{Z} = \boldsymbol{S}^T \begin{bmatrix} \boldsymbol{T}_1 + \frac{\eta_2}{\eta_1} \boldsymbol{T}_2 & -\boldsymbol{K}_1 - \boldsymbol{K}_2 \\ \boldsymbol{K}_1 + \boldsymbol{K}_2 & \boldsymbol{T}_1 + \frac{\eta_1}{\eta_2} \boldsymbol{T}_2 \end{bmatrix} \boldsymbol{S}. \tag{13}$$

And $\boldsymbol{S}$ denotes the permutation matrix that mixes the components of $\boldsymbol{I}^J$ and $\boldsymbol{I}^M$ into $\boldsymbol{I}$. In what follows, $\boldsymbol{Z}$ is termed the reordered interaction matrix. The recursive decomposition of Γ and unknown/field reordering procedures induce a hierarchical partitioning of the interaction matrix $\boldsymbol{Z}$ that is illustrated in Figure 1 for $L^{\text{M}} = 7$ and Γ modeled by a 2D curve.

Step (ii) classically computes blocks representing near-field interactions via Equations 10 and 11 and butterfly-compresses blocks representing far-field interactions. Consider a $m \times n$ level-l far-field block $\boldsymbol{Z}_s^O$ in $\boldsymbol{Z}$ with $n \approx m \approx$

TABLE 1 The technical data for the setups and solutions of the largest scattering problems considered in this paper

	Sphere	Almond	Helicopter
Max dimension	2 m (20 λ)	25 cm (33 λ)	22 m (36 λ)
Unknown N	961 008	722 712	559 992
Memory: Z	493.1 GB	162.3 GB	111.5 GB
Memory: LU factor	853.5 GB	348.1 GB	383.1 GB
Matrix filling time	794 s	1.6 h	535 s
Factorization time	82.6 h	26.6 h	60 h
Solution time	136 s	37 s	65 s

$N/2^l$. Note that odd/even indices in set S point to electric/magnetic unknowns I_n^J/I_n^M; similarly odd/even indices in set O point to measured fields in V_n^E/V_n^M. The butterfly scheme first divides $\boldsymbol{Z}_s^O$ into judiciously-selected submatrices $\boldsymbol{Z}_{S_i^d}^{O_j^d}$: for each $0 \le d \le L=L^M-l$, $i=1,\ldots,2^{L-d}$, $j=1,\ldots,2^{d_i}$, S_i^d and O_j^d are subsets corresponding to level-$l-L+d$ and level-$(l-d)$ subscatterers, respectively. It can be shown that the (butterfly) rank r of each submatrix $\boldsymbol{Z}_{S_i^d}^{O_j^d}$ is approximately constant.[23] Upon computing LR approximations to all 2^L $(L+1)$ submatrices, the butterfly representation $\boldsymbol{B}$ of $\boldsymbol{Z}_S^O$ consists of the product of $L+2$ sparse matrices

$$\boldsymbol{B}=\boldsymbol{P}\boldsymbol{R}_L\ldots\boldsymbol{R}_1\boldsymbol{Q} \tag{14}$$

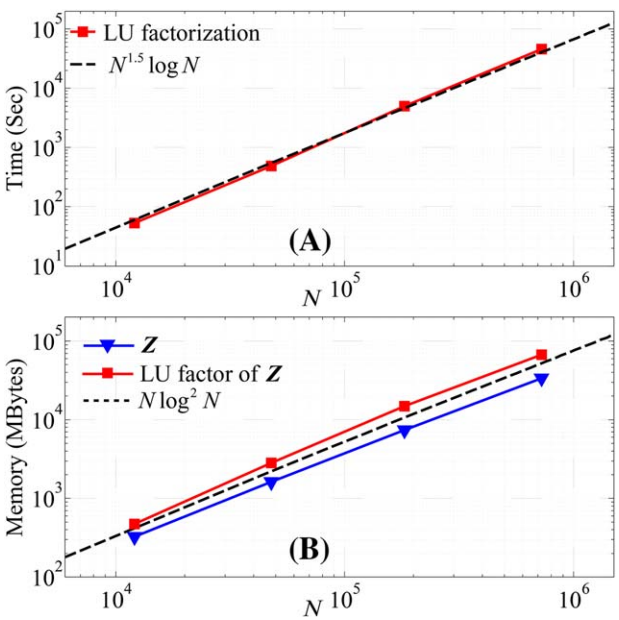

FIGURE 2 (A) Memory costs for storing $\boldsymbol{Z}$ and its LU factorization and (B) CPU times for the factorization phase using the proposed solver [Color figure can be viewed at wileyonlinelibrary.com]

where $\boldsymbol{P}$ and $\boldsymbol{Q}$ are block diagonal projection matrices, and the interior matrices $\boldsymbol{R_d}$, $d=1,\ldots,L$ are also block diagonal after (predefined) row permutation:

$$\boldsymbol{P}=\mathrm{diag}(\boldsymbol{P}_1,\ldots,\boldsymbol{P}_{2^L}) \tag{15}$$

$$\boldsymbol{Q}=\mathrm{diag}(\boldsymbol{Q}_1,\ldots,\boldsymbol{Q}_{2^L}) \tag{16}$$

$$\boldsymbol{D}_d\boldsymbol{R}_d=\mathrm{diag}(\boldsymbol{R}_{d,1},\ldots,\boldsymbol{R}_{d,2^{L-1}}) \tag{17}$$

Here, $\boldsymbol{D_d}$ is the permutation matrix that yields $\boldsymbol{R_d}$ block diagonal, and the diagonal blocks in Equations 15, 16, and 17 have approximate dimensions $(m/2^L)\times r$, $r\times(n/2^L)$, and $r\times 2r$ respectively (Figure 1).

It can be shown that construction and storage of one submatrix $\boldsymbol{Z}_S^O$ requires only $O(n \log n)$ CPU and memory resources, and that the overall memory and CPU requirements associated with the matrix filling phase scale as $O(N\log^2 N)$.

2.3 | Hierarchical LU factorization

The second phase of the proposed solver constructs a butterfly-compressed hierarchical LU factorization of the reordered interaction matrix. The crux of the factorization process relies on the experimental observation that all blocks in the LU factors dimension-wise matching far-field blocks in $\boldsymbol{Z}$ are butterfly compressible with similar butterfly ranks. The solver arrives at a compressed representation of the LU factors of $\boldsymbol{Z}$ using randomized butterfly reconstruction methods to represent compositions of existing butterflies (additions, multiplications, and solutions of triangular systems) in terms of new butterflies.

The factorization process starts by partitioning and LU factorizing the impedance matrix $\boldsymbol{Z}$ as

$$\boldsymbol{Z}=\begin{bmatrix}\boldsymbol{Z}_{11} & \boldsymbol{Z}_{12}\\ \boldsymbol{Z}_{21} & \boldsymbol{Z}_{22}\end{bmatrix}=\begin{bmatrix}\boldsymbol{L}_{11} & \\ \boldsymbol{L}_{21} & \boldsymbol{L}_{22}\end{bmatrix}\begin{bmatrix}\boldsymbol{U}_{11} & \boldsymbol{U}_{12}\\ & \boldsymbol{U}_{22}\end{bmatrix} \tag{18}$$

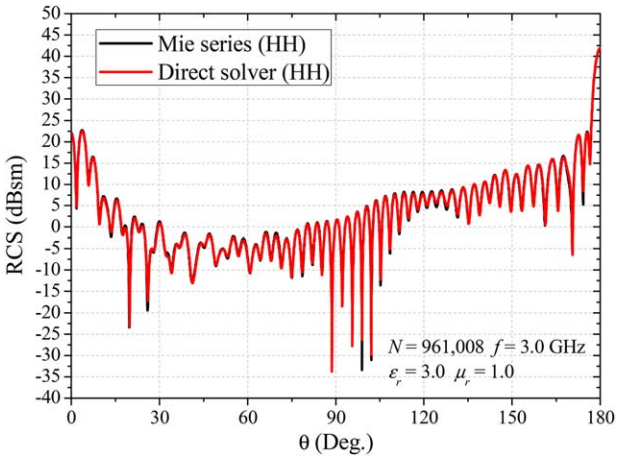

FIGURE 3 HH bistatic RCS of the sphere at 3 GHz computed at $\theta = 90°$ and $\varphi = [0,180]°$ using the proposed solver and the Mie series [Color figure can be viewed at wileyonlinelibrary.com]

The process proceeds as follows: (i) LU factorize $\boldsymbol{Z}_{11} = \boldsymbol{L}_{11}\boldsymbol{U}_{11}$; (ii) compute $\boldsymbol{U}_{12}=\boldsymbol{L}_{11}^{-1}\boldsymbol{Z}_{12}$ via back substitution; (iii) compute $\boldsymbol{L}_{21}=\boldsymbol{Z}_{21}\boldsymbol{U}_{11}^{-1}$ via back substitution; (iv) update $\hat{\boldsymbol{Z}}_{22}=\boldsymbol{Z}_{22}-\boldsymbol{L}_{21}\boldsymbol{U}_{12}$; and (v) LU factorize $\hat{\boldsymbol{Z}}_{22}=\boldsymbol{L}_{22}\boldsymbol{U}_{22}$. The constituent blocks in these five procedures are further partitioned until $\boldsymbol{Z}_{11}$, $\boldsymbol{Z}_{12}$, $\boldsymbol{Z}_{21}$, $\boldsymbol{L}_{21}/\boldsymbol{U}_{12}$, $\hat{\boldsymbol{Z}}_{22}$ in steps (i)–(v) dimension-wise match those in $\boldsymbol{Z}$. Consequently, the hierarchical partitioning of the LU factors of $\boldsymbol{Z}$ matches exactly that of $\boldsymbol{Z}$ (Figure 1).

During the recursive factorization process (i)–(v), there are essentially three types of block operations that are not recursive in nature:

$$\boldsymbol{B}=\boldsymbol{B}_1+\boldsymbol{B}_2 \tag{19}$$

$$\boldsymbol{B}=\boldsymbol{B}_1.\boldsymbol{A} \text{ or } \boldsymbol{B}=\boldsymbol{A}.\boldsymbol{B}_1 \tag{20}$$

$$\boldsymbol{B}=\hat{\boldsymbol{L}}^{-1}.\boldsymbol{B}_1 \text{ or } \boldsymbol{B}=\boldsymbol{B}_1.\boldsymbol{U}^{-1} \tag{21}$$

Here, $\boldsymbol{B}_1$ and $\boldsymbol{B}_2$ are butterfly-compressed matrices, and $\boldsymbol{A}$, $\hat{\boldsymbol{L}}$ and $\hat{\boldsymbol{U}}$ are hierarchical partitioned full, lower triangular, and upper triangular matrices with butterfly-compressed blocks. It is assumed and experimentally observed that all $\boldsymbol{B}$'s in Equations 19–21 that dimension-wise match far-field blocks in $\boldsymbol{Z}$ can be butterfly-compressed. To arrive at butterfly approximations for all $\boldsymbol{B}$'s, the solver uses a fast randomized scheme that relies on the information gathered by (rapidly) multiplying $\boldsymbol{B}$ (i.e. the right hand sides in Equations 19–21) and its transpose to sparse random vectors.[21]

The memory requirement of the factorization step scales as $O(N \log^2 N)$ due to the observation that butterfly ranks in Equations 19–21 are approximately constant; the computational cost of the factorization step scales as $O(N^{1.5} \log N)$ because each randomized butterfly operation Equations 19–21 requires $O(n^{1.5} \log n)$ CPU time. A detailed complexity analysis can be found in Ref. [21].

Once factorized, the inverse of the impedance matrix can be rapidly applied to excitation vectors using partitioned forward/backward substitution.[3]

3 | NUMERICAL RESULTS

This section presents numerical results that demonstrate the efficiency and accuracy of the proposed solver. Simulations are performed on a cluster of eight-core 2.60 GHz Intel Xeon

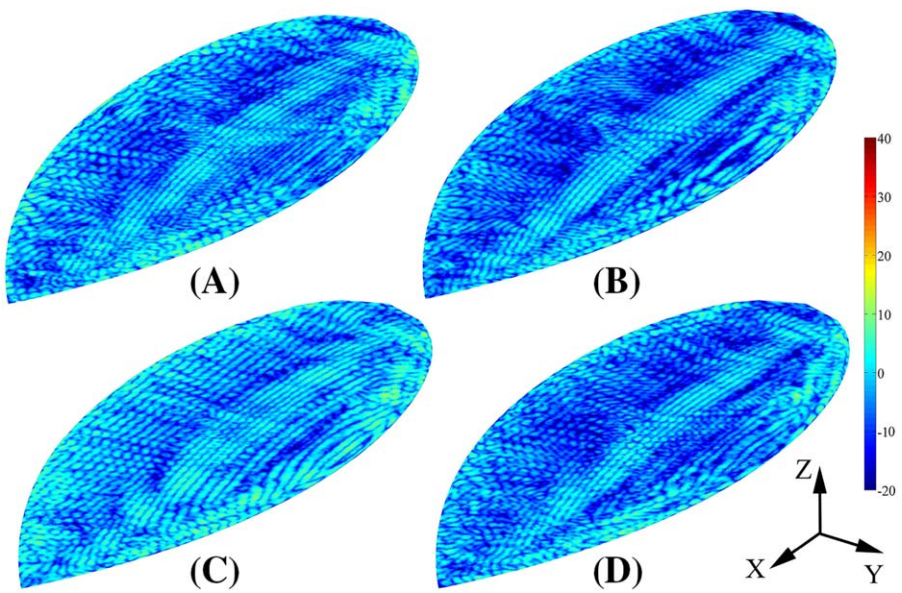

FIGURE 4 Current density (in dB) induced on the almond computed by the proposed direct solver: (A) $\eta_1\boldsymbol{J}$ and (B) $\boldsymbol{M}$ induced by a x-polarized and-y-propagating incident electric field, and (C) $\eta\boldsymbol{J}$ and (D) $\boldsymbol{M}$ induced by a z-polarized and-y-propagating incident electric field [Color figure can be viewed at wileyonlinelibrary.com]

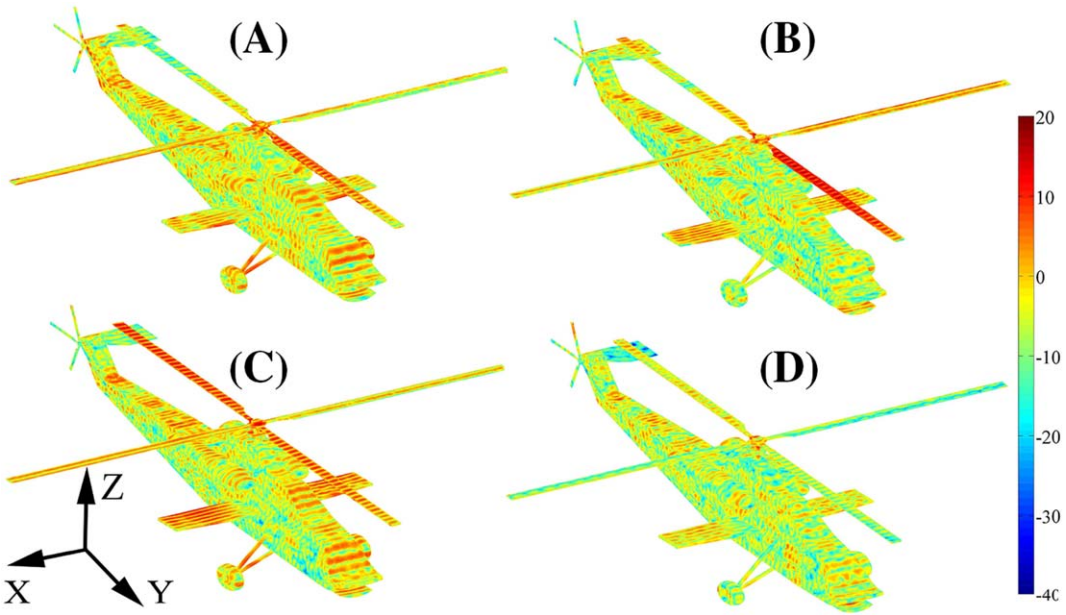

FIGURE 5 Current density (in dB) induced on the helicopter computed by the proposed direct solver: (A) $\eta_1 \boldsymbol{J}$ and (B) $\boldsymbol{M}$ induced by a x-polarized and-y-propagating incident electric field, and (C) $\eta \boldsymbol{J}$ and (D) $\boldsymbol{M}$ induced by a z-polarized and-y-propagating incident electric field [Color figure can be viewed at wileyonlinelibrary.com]

E5–2670 processors with 4 GB memory per core. In all examples, region 1 is vacuum, i.e. $\varepsilon_1 = \varepsilon_0$ and $\mu_1 = \mu_0$, the permittivity and permeability of the scatterers are $\varepsilon_2 = 3\varepsilon_0$ and $\mu_2 = \mu_0$, and χ is set to 2.

3.1 | Sphere

First, the memory and CPU requirements of the proposed solver are verified via its application to the analysis of scattering from a 1 m-radius dielectric sphere. The frequency $f = \omega/(2\pi)$ and number of unknowns N are changed from 0.4 GHz and 12 072 to 3.2 GHz and 725 274, respectively. The solver utilizes 16 processors. The memory required to store $\boldsymbol{Z}$ and its LU factors, plotted in Figure 2A, scale as $O(N \log^2 N)$. The CPU time required for factorizing $\boldsymbol{Z}$, shown in Figure 2B, clearly adheres to the predicted $O(N^{1.5} \log N)$ scaling law.

Next, the accuracy of the proposed solver is demonstrated via computation of the sphere's bistatic radar cross section (RCS) for $f = 3$ GHz and $N = 961\,008$. Matrix $\boldsymbol{Z}$ is hierarchically partitioned using 10 levels after setting the finest-level block dimension to approximately 938. The memory required for storing $\boldsymbol{Z}$ and its LU factors, and the CPU time required for filling and factorizing $\boldsymbol{Z}$ are listed in Table 1. The solver requires peak memory of 853 GB and total CPU time of 82.6 hours on 64 processors. The HH-polarized bistatic RCS in directions along $\theta = 90°$ and $\varphi = [0,180]°$ for a total of 10 000 directions are computed and compared with the Mie series solutions in Figure 3. Results agree very well.

3.2 | NASA almond

Next, the proposed solver is applied to the analysis of scattering from a NASA almond enclosed by a fictitious box of dimensions 25.25 cm × 9.76 cm × 3.25 cm. The almond is illuminated by a $f = 40.0$ GHz plane wave that is either x- or z-polarized and propagating along y. Matrix $\boldsymbol{Z}$ with $N = 722\,712$ is partitioned using 9 levels by setting the finest-level block dimension to approximately 1411. The solver requires peak memory of 348 GB and total CPU time of 26.6 hours using 64 processors (see Table 1). The electric and magnetic currents induced on the almond are plotted in Figure 4.

3.3 | Helicopter

Finally, the proposed solver is applied to the analysis of scattering from a "plastic helicopter" model residing in a fictitious box of dimensions 18.60 m × 21.96 m × 7.15 m. The helicopter is illuminated by a $f = 0.5$ GHz plane wave that is either x- or z-polarized and propagating along the y direction. The impedance matrix with $N = 559\,992$ is hierarchically partitioned with 10 levels upon setting the size of the finest-level block dimension to approximately 546. The memory requirements for storing $\boldsymbol{Z}$ and its LU factorization, and the

CPU times for filling and factorizing $\boldsymbol{Z}$ as well as the back-substitution phases are listed in Table 1. The solver requires 383.1 GB memory and 60 hours CPU time using 64 processors. The electric and magnetic currents on the helicopter are shown in Figure 5.

4 | CONCLUSIONS

A fast butterfly-based LU factorization scheme for solving the PMCHWT equations pertinent to the analysis of scattering from electrically large homogenous dielectric-magnetic objects was presented. The proposed solver reorders and butterfly-compresses blocks in the interaction matrix and its LU factors. Importantly, the observed CPU and memory complexities of the resulting solver scale as $O(N^{1.5} \log N)$ and $O(N \log^2 N)$, respectively. Current efforts are aimed at reducing the leading constants implicit in the above estimates, to allow application of the solver to much bigger objects.

ORCID

Yang Liu http://orcid.org/0000-0003-3750-1178

REFERENCES

[1] Yla-Oijala P, Taskinen M, Jarvenpaa S. Analysis of surface integral equations in electromagnetic scattering and radiation problems. *Eng Anal Bound Elem.* 2008;32:196–209.

[2] Song J, Lu C-C, Chew WC. Multilevel fast multipole algorithm for electromagnetic scattering by large complex objects. *IEEE Trans Antennas Propag.* 1997;45:1488–1493.

[3] Bebendorf M. Hierarchical LU decomposition-based preconditioners for BEM. *Computing.* 2005;74(3):225–247.

[4] Shaeffer J. Direct solve of electrically large integral equations for problem sizes to 1 M unknowns. *IEEE Trans Antennas Propag.* 2008;56:2306–2313.

[5] Chai W, Jiao D. An-matrix-based integral-equation solver of reduced complexity and controlled accuracy for solving electrodynamic problems. *IEEE Trans Antennas Propag.* 2009;57:3147–3159.

[6] Greengard L, Gueyffier D, Martinsson P-G, Rokhlin V. Fast direct solvers for integral equations in complex three-dimensional domains. *Acta Numerica.* 2009;18:243–275.

[7] Heldring A, Rius JM, Tamayo JM, Parron J, Ubeda E. Multiscale compressed block decomposition for fast direct solution of method of moments linear system. *IEEE Trans Antennas Propag.* 2011;59:526–536.

[8] Guo H, Hu J, Shao H, Nie Z. Hierarchical matrices method and its application in electromagnetic integral equations. *Int J Antennas Propag.* 2012;2012:1.

[9] Wei J-G, Peng Z, Lee J-F. A fast direct matrix solver for surface integral equation methods for electromagnetic wave scattering from non-penetrable targets. *Radio Sci.* 2012;47(5).

[10] Corona E, Martinsson P-G, Zorin D. An O(N) direct solver for integral equations on the plane. *Appl Comput Harmon Anal.* 2015;38:284–317.

[11] Michielssen E, Boag A, Chew W. Scattering from elongated objects: direct solution in O(N log 2 N) operations. *IEE Proc Microw Antennas Propag.* 1996;143(4):277–283.

[12] Martinsson P-G, Rokhlin V. A fast direct solver for scattering problems involving elongated structures. *J Comput Phys.* 2007;221:288–302.

[13] Winebrand E, Boag A. A multilevel fast direct solver for EM scattering from quasi-planar objects. *Proc Int Conf Electromagn Adv Appl IEEE.* 2009;640–643.

[14] Brick Y, Lomakin V, Boag A. Fast direct solver for essentially convex scatterers using multilevel non-uniform grids. *IEEE Trans Antennas Propag.* 2014;62:4314–4324.

[15] Michielssen E, Boag A. A multilevel matrix decomposition algorithm for analyzing scattering from large structures. *IEEE Trans Antennas Propag.* 1996;44:1086–1093.

[16] Candes E, Demanet L, Ying L. A fast butterfly algorithm for the computation of Fourier integral operators. *Multiscale Model Simul.* 2009;7:1727–1750.

[17] O'neil M, Woolfe F, Rokhlin V. An algorithm for the rapid evaluation of special function transforms. *Appl Comput Harmon Anal.* 2010;28:203–226.

[18] Tygert M. Fast algorithms for spherical harmonic expansions, III. *J Comput Phys.* 2010;229:6181–6192.

[19] Liu Y, Guo H, Michielssen E. A HSS matrix-inspired butterfly-based direct solver for analyzing scattering from two-dimensional objects. *IEEE Antennas Wirel Propag Lett.* 2016.

[20] Guo H, Hu J, Michielssen E. On MLMDA/butterfly compressibility of inverse integral operators. *IEEE Antennas Wirel Propag Lett.* 2013;12:31–34.

[21] Guo H, Liu Y, Hu J, Michielssen E. A butterfly-based direct integral equation solver using hierarchical LU factorization for analyzing scattering from electrically large conducting objects. *IEEE Trans Antennas Propag.* 2016;65:4742–4750.

[22] Rao SM, Wilton DR, Glisson AW. Electromagnetic scattering by surfaces of arbitrary shape. *IEEE Trans Antennas Propag.* 1982;30:409–418.

[23] Bucci OM, Franceschetti G. On the degrees of freedom of scattered fields. *IEEE Trans Antennas Propag.* 1989;37:918–926.

How to cite this article: Guo H, Liu Y, Jun H, Michielssen E. A butterfly-based direct solver using hierarchical LU factorization for Poggio-Miller-Chang-Harrington-Wu-Tsai equations. *Microw Opt Technol Lett*. 2018;60:1381–1387. https://doi.org/10.1002/mop.31166